A MTPA Control Strategy for Mono-Inverter Multi-PMSM System

Tianyi Liu, Maurice Fadel, Jun Li, Xiaoyan Ma

A MTPA Control Strategy for Mono-Inverter Multi-PMSM System

Tianyi Liu, Maurice Fadel, Jun Li, Xiaoyan Ma

***Abstract*—Making electrical driving systems cheaper, lighter, and more reliable is the consistent pursuit of current research and development. Mono-inverter multipermanent magnet synchronous motor systems tend to share the static converters in electromechanical systems by connecting machines in parallel. This type of system has an obvious advantage in overall weight and cost. In this article, we have proposed a new maximum torque per ampere (MTPA) control strategy for a MIMPMSM system, which supports three or more machines in parallel and works both in motor mode and brake mode. The calculation of the MTPA point minimizing the overall joule loss of the system is also given. The synchronization condition, stability, and optimal efficiency of the system are strictly proven. This new control structure is simple making current single PMSM systems easy to upgrade to support the MIMPMSM system. The experiment has demonstrated its feasibility, stability, and improvements in efficiency.**

***Index Terms*—Efficiency, multi-PMSM, stability.**

I. Introduction

THE idea of connecting machines in parallel in a multi-machines system has been proposed decades ago, as the demand for reducing the number of components for an electrical system is conventional. This idea has been successfully introduced to a multi-induction machine (IM) system and applied to the various purposes such as train traction [1], electric vehicle propulsion [2].

This idea is also introduced into a multipermanent magnet synchronous machine (PMSM) system with the popularity of PMSM, for seeking improvement in the system dynamic and efficiency. In some applications, such as cooling fan [3] or pump driving [4], multiple PMSMs are performing the same task, usually with the same speed in steady state while less dynamic performance is required [5]. Considering that PMSM is synchronous to the inverter voltage frequency, they can also be connected in parallel to share the same inverter, which attracts many researchers' interest.

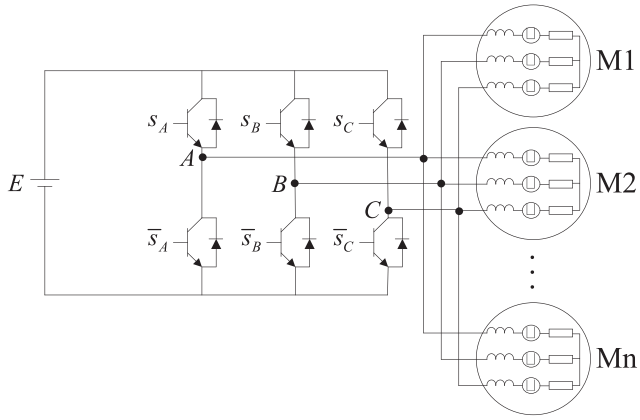

Fig. 1. n-PMSM connect to a 2-level 3-leg inverter.

A parallel IM system is naturally stable because IM's torque is proportional to its slip-speed. While a parallel PMSM system (see Fig. 1) has an inherent stability problem. In previous studies, researchers decided to start with the simplest case of such a system: 2 machines, which is called mono-inverter dual-PMSM system (MIDPMSM), to explore the possibility of controlling it. Among these research works, in [6]–[11], the authors have proposed to use the average value of the speed, position, and current of two machines. Besides, the *master–slave* strategy [12]–[15], tends to control only one of the two machines. On the other hand, model predictive control (MPC) [16]–[18] also gives another possible solution to the control problem. The feasibility, controllability of these control strategies have been well verified [19]–[20]. Moreover, the efficiency optimization problem of a MIDPMSM system that minimizes the joules losses is also studied in [13] and [14]. The feasibility, controllability, and efficiency problem of this system have been well studied but under the following limitations:

1) only two machines can be connected parallelly;
2) machines only work in motor region.

These limitations have created some obstacles in putting the multi-PMSMs system into practice, because in actual application, such as cooling fan, pump driving, or conveyor belt, it may happen that more than two machines are needed. This limits the possibility to further reduce the electric components in the system.

Manuscript received June 1, 2020; revised September 30, 2020; accepted November 11, 2020. Date of publication November 17, 2020; date of current version February 5, 2021. Recommended for publication by Associate Editor E. Armando. *(Corresponding author: Xiaoyan Ma.)*

Tianyi Liu and Jun Li are with the School of Aerospace Engineering and Applied Mechanics, Tongji University, Shanghai 200092, China (e-mail: tianyi.liu@tongji.edu.cn; muziyi@tongji.edu.cn).

Maurice Fadel is with the Universit´e de Toulouse, Institut national Polytechnique de Toulouse, Universit´e Paul Sabatier, Laboratoire Plasma et Conversion d'Energie, 31071 Toulouse, France (e-mail: maurice.fadel@laplace.univ-tlse.fr).

Xiaoyan Ma is with the College of Architecture and Urban Planning, Tongji University, Shanghai 200092, China (e-mail: xiaoyan_ma@tongji.edu.cn).

The brake condition is not well addressed in the current parallel-PMSM research works, which is required in high inertial application or energy recovering [24]–[26]. This insufficiency limits the working range and makes the system risky or unstable. In a single PMSM system, the brake mechanism is not mandatory if slowing down passively (i.e., by mechanical brake) is acceptable. But, for a MIMPMSM system, the load and friction conditions are not the same to all machines. These machines will slow down at different speed and the system loses synchronization. Also, it would be interesting to extend such a system to multigenerator applications, such as wind turbines [27]–[28], multiple generators can share the same ac–dc inverter then connect to the grid.

Meanwhile, some research works have contributed to the control problem of a general parallel-PMSM system, monoinverter multi-PMSM (MIMPMSM) system, when more than two machines are involved. In [21], Yamada *et al.* have proposed an interesting idea to this problem by using an amplitude modulation technique. But the demodulation network, which requires high power inductance and capacitor, also increases the total weight of the system and makes a drawback in the initial purpose of a parallel PMSM system. Nagano *et al.* [22] have used the open-loop *V/f* control method. Each machine is equipped with damping winding to solve the in-stable problem of the *V/f* method. A small auxiliary inverter is connected to the damping winding to create a damping effect. In [23], Liu and Fadel have proposed a control strategy to the MIMPMSM system without modifying or adding electrical components. This article is very basic as it only gives a simulation test. The actual feasibility, stability, robustness, and performance of this proposition are still unclear.

In this article, we proposed a new maximum torque per ampere (MTPA) control strategy for a MIMPMSM system, which works both in motor mode and brake mode. Its principle, synchronization condition, stability, robustness, dynamic performance, and efficiency are well expounded and verified by experiment.

This article is organized as follows: In Section II, the steady-state model of a general MIMPMSM is defined, then the control characteristic is discussed through constraint analysis of the steady-state model. In Section III, the control strategy is presented. Its synchronization condition, stability, robustness, and efficiency problem are addressed. Section IV presents various experimental test to the proposed control strategy to illustrate its stability, robustness, and effectiveness of the efficiency optimization.

II. Control Characteristic of a MIMPMSM System

The controller designed in this article bases on the steady-state model of a MIMPMSM system. It must be defined before proceeding to the analysis. Then, though analyzing the model structure, the control variable of the control strategy is determined.

A. Steady-State Model of the MIMPMSM System

In this model, a nonsalient pole PMSM that has sinusoidal electromotive force is considered. The magnetic loss and cogging torque are neglected. Consider that there are N ($N \geq 3$) machines involved in the system, each machine is assigned with a unique index from 1 to N and represented by $\mathrm{M}_1 \cdots \mathrm{M}_N$. Defining the d axis of a *d-q* coordinate aligns with the flux of the rotor, the steady-state model of M_1 can be expressed as

$$\begin{bmatrix} \boldsymbol{V_{d1}} \\ \boldsymbol{V_{q1}} \end{bmatrix} = \begin{bmatrix} \boldsymbol{R_s} & -\boldsymbol{L_s\omega_e} \\ \boldsymbol{L_s\omega_e} & \boldsymbol{R_s} \end{bmatrix} \begin{bmatrix} \boldsymbol{I_{d1}} \\ \boldsymbol{I_{q1}} \end{bmatrix} + \begin{bmatrix} 0 \\ \boldsymbol{\omega_e\varphi_p} \end{bmatrix} \quad (1)$$

where

V_d, V_q: stator Voltage in *d-q* frame;
I_d, I_q: stator Current in *d-q* frame;
L_s: stator phase windings inductance;
φ_{p}: permanent magnets flux;
R_s: stator phase resistance;
ω_{e}: electrical speed.

The electrical torque is then given as

$$\boldsymbol{T_{e1}} = \boldsymbol{N_p\varphi_p I_{q1}}. \quad (2)$$

For anyone of the rest machines, which is expressed by $\mathrm{M_k}, \mathrm{k} \in [2, \mathrm{N}]$, $\tilde{\mathrm{V}}_{\mathrm{dq}}$ must be mapped into its coordinate since there is electrical angle displacement between two machines. To define $\theta_{\mathrm{dk}} = \theta_{\mathrm{k}} - \theta_1$, where θ_1 and θ_{k} correspond to the electrical angle of each machine, the steady-state model of $\mathrm{M_k}$ can be expressed as

$$\begin{bmatrix} \cos\boldsymbol{\theta_{dk}} & \sin\boldsymbol{\theta_{dk}} \\ -\sin\boldsymbol{\theta_{dk}} & \cos\boldsymbol{\theta_{dk}} \end{bmatrix} \begin{bmatrix} \boldsymbol{V_{d1}} \\ \boldsymbol{V_{q1}} \end{bmatrix} = \begin{bmatrix} \boldsymbol{R_s} & -\boldsymbol{L_s\omega_e} \\ \boldsymbol{L_s\omega_e} & \boldsymbol{R_s} \end{bmatrix} \begin{bmatrix} \boldsymbol{I_{dk}} \\ \boldsymbol{I_{qk}} \end{bmatrix} + \begin{bmatrix} 0 \\ \boldsymbol{\omega_e\varphi_p} \end{bmatrix}. \quad (3)$$

Consider that in actual applications described in this article, the same types of PMSMs are usually used, it is assumed that all machines have the same parameters and operate at the same speed in steady state. By merging model of $\mathrm{M_1} \sim \mathrm{M_N}$, the steady-state model of a MIMPMSM system can be obtained (4) shown at the bottom of this page.

$$\begin{bmatrix} 1 & 0 \\ 0 & 1 \\ \cos\theta_{d2} & \sin\theta_{d2} \\ -\sin\theta_{d2} & \cos\theta_{d2} \\ \vdots & \vdots \\ \cos\theta_{dN} & \sin\theta_{dN} \\ -\sin\theta_{dN} & \cos\theta_{dN} \end{bmatrix}_{2\times 2N} \begin{bmatrix} V_{d1} \\ V_{q1} \end{bmatrix} = \begin{bmatrix} R_s & -L_s\omega_e & \cdots & 0 & 0 \\ L_s\omega_e & R_s & \cdots & 0 & 0 \\ \vdots & \vdots & \ddots & \vdots & \vdots \\ 0 & 0 & \cdots & R_s & -L_s\omega_e \\ 0 & 0 & \cdots & L_s\omega_e & R_s \end{bmatrix}_{2N\times 2N} \begin{bmatrix} I_{d1} \\ I_{q1} \\ \vdots \\ I_{dN} \\ I_{qN} \end{bmatrix}_{1\times 2N} + \begin{bmatrix} 0 \\ \omega_e\varphi_p \\ \vdots \\ 0 \\ \omega_e\varphi_p \end{bmatrix}_{1\times 2N} \quad (4)$$

Due to the structure of a 2-level 3-legs inverter, the leg is either connected to V_{dc} or 0. The dc bus is thought to have enough capacity that supplies or absorbs the power. This means that machines are fully decoupled, there is not power circulation among machines.

B. Control Variable Selection

The control variable selection problem is essential in a MIMPMSM system as strong coupling presents in it. Here, the constraint analysis method is used. Control is feasible when and only voltage solution exists for desired torque ($I_{q1} \dots I_{qN}$) and speed (ω_e). For example, in a single PMSM system (1), the torque (I_{q1}) is a known variable in it, which is determined passively by actual state of the machine. Then, it still has three unknown variables (V_{d1}, V_{q1}, I_{d1}) but only two equations are presented. This means that, for a given torque, there are infinity solutions of these unknown variables. The system is underconstrained. In a MTPA operation, I_{d1} is set to 0, which is an additional constraints applied to (1) make the steady-state model properly constrained and V_{d1}, V_{q1} becomes unique.

Back into the case of a MIMPMSM system, in (4) there are $2N + 1$ unknown variables including $\underbrace{V_{d1}, V_{q1}}_{2}$, $\underbrace{I_{d1}, \dots, I_{d1}}_{N}$, $\underbrace{\theta_{d2}, \dots, \theta_{dN}}_{N-1}$, while $2N$ equations are provided. In this case, I_{d1} is chosen to be the control variable so that the system is properly constrained and the resulted controller structure would be simpler.

III. Control Strategy Design

Based on the analysis in the previous section, the controller is designed as that one of the machines is controlled closed-loop (master machine) and other machines are left open-loop (slave machines) to meet up with the steady-state constraints. With such a configuration, considering that a PMSM is open-loop stable only when its synchronization condition is satisfied, the synchronization condition of a MIMPMSM system is studied in the first place. Then, the stability of all open-loop machine is studied based on the small signal model. In the last, the control strategy is designed based on these conclusions.

A. Synchronization Condition of an Open-Loop PMSM

In open-loop operation, the controller must provide enough voltage to compensate the back EMF and voltage drop on the stator resistance so that the generated torque is larger than its load. Otherwise, the machine will lose synchronization [29]. As all machines are paralleled connected in a MIMPMSM system, this voltage must consequently satisfy all machines' requirement so that the synchronization condition is achieved.

In the first step, the synchronization condition of an open-loop PMSM is mathematically described. As the inverter voltage is the only linkage between machines, this condition is expressed with the relationship to the voltage and then converted to I_{d1} so that it can be regulated to make all machine synchronized.

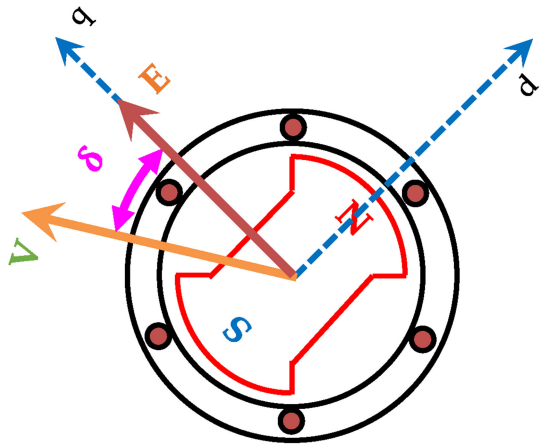

Fig. 2. Relationship of $\boldsymbol{\delta}$ angle.

Fig. 2 represents a simple vector diagram of a PMSM. The *d*-axis is aligned with rotor's flux. *V* is the applied voltage vector and E is the back-EMF vector. The angle between *V* and *E* is denoted as δ. Then, the steady-state model of a PMSM with respect to δ can be obtained as

$$\begin{aligned}\begin{bmatrix} \boldsymbol{V_d} \\ \boldsymbol{V_q} \end{bmatrix} &= \begin{bmatrix} -|\boldsymbol{V}| \sin \boldsymbol{\delta} \\ |\boldsymbol{V}| \cos \boldsymbol{\delta} \end{bmatrix} \\ &= \begin{bmatrix} \boldsymbol{R_s} & -\boldsymbol{L_s \omega_e} \\ \boldsymbol{L_s \omega_e} & \boldsymbol{R_s} \end{bmatrix} \begin{bmatrix} \boldsymbol{I_d} \\ \boldsymbol{I_q} \end{bmatrix} + \begin{bmatrix} 0 \\ \boldsymbol{\omega_e \varphi_p} \end{bmatrix}. \end{aligned} \tag{5}$$

According to (5), the torque relationship with respect to δ and *V* can be described as

$$\boldsymbol{T_e} = \boldsymbol{N_p \varphi_p} \frac{|\boldsymbol{V}|}{\boldsymbol{Z}} \cos\left(\boldsymbol{\delta} - \tan^{-1} \frac{\boldsymbol{\omega_e L_s}}{\boldsymbol{R_s}}\right) - \boldsymbol{N_p \varphi_p} \frac{\boldsymbol{R_s \omega_e \varphi_p}}{\boldsymbol{Z}^2} \tag{6}$$

where

$$\boldsymbol{Z} = \sqrt{\boldsymbol{R_s}^2 + (\boldsymbol{L_s \omega_e})^2}\,. \tag{7}$$

T_e corresponds to the torque of the PMSM. When $T_e > 0$, the machine works in a motor mode, when $T_e < 0$, the machine works in a brake mode. Fig. 3 shows an example curve of (6). Suppose that a PMSM is running at steady state (indicated as operation point A), a change in torque angle $\Delta\delta$ away from equilibrium will result in a torque change ΔT_e, which can be described by

$$\Delta\, \boldsymbol{T_e} = \boldsymbol{K_e}\, \Delta \boldsymbol{\delta}. \tag{8}$$

When $K_e > 0$, the machine remains synchronized when positive rotating [30]. Obviously, (8) only valid when the applied torque does not exceed the maximum torque point, otherwise the machine will lose synchronization (operation point C). From (6), the maximum and minimum value of T_e can be obtained, which are

$$\boldsymbol{T_e^{\max}} = \boldsymbol{T_e^n} + \boldsymbol{N_p \varphi_p} \frac{|\boldsymbol{V}|}{\boldsymbol{Z}} \tag{9}$$

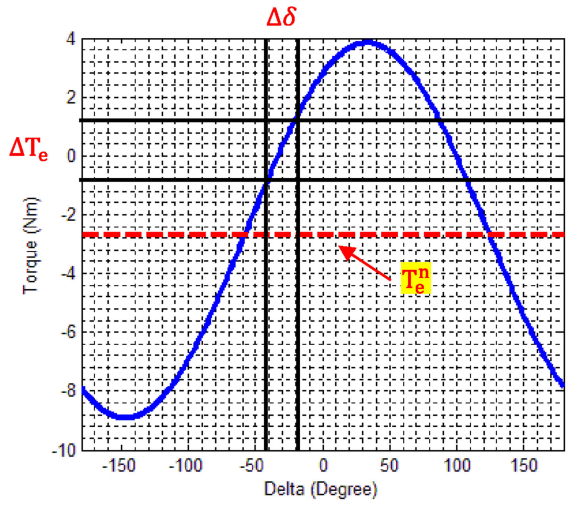

Fig. 3. Torque curve with respect to $\boldsymbol{\delta}$.

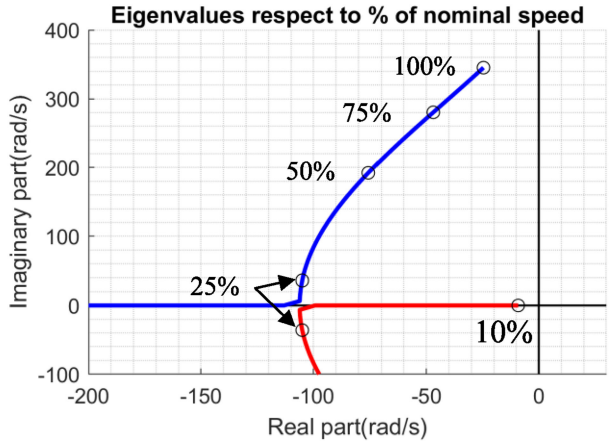

Fig. 4. Eigenvalues of an open-loop PMSM with respect to different speed.

and

$$\boldsymbol{T_e^{\min} = T_e^n - N_p\varphi_p \frac{|V|}{Z}} \tag{10}$$

with

$$\boldsymbol{T_e^n = -N_p\varphi_p \frac{R_s\omega_e\varphi_p}{Z^2}}\,. \tag{11}$$

A PMSM's synchronization condition is satisfied only when

$$\boldsymbol{T_e^{\min} \le T_e \le T_e^{\max}}\,. \tag{12}$$

According to (9), (10), and (12), the synchronization condition of a PMSM with respect to its voltage magnitude can be described as

$$\boldsymbol{|V| \ge \frac{Z}{N_p\varphi_p}|T_e - T_e^n|} \tag{13}$$

which is valid for both motor and brake regions of a PMSM.

Moreover, $\mathrm{T_e^n}$ corresponds to the power neutral point of a PMSM torque when three phases are short connected. The detailed derivation and proof of this conclusion can be found in Appendix A.

B. Synchronization Condition of a MIMPMSM System

For a MIMPMSM system, other than the closed-loop controlled $\mathrm{M_1}$, $\mathrm{T_e}$-δ curve presented in Fig. 3 is valid for all open-loop machines. Because all parallel connected machines have the same $|\mathrm{V}|$. Thus, the synchronization condition of a MIMPMSM system is satisfied when all machines' torque is within the maximum torque point, that is

$$\boldsymbol{T_e^{\min} \le T_{ek} \le T_e^{\max},\ k \in [2, N]} \tag{14}$$

where $\mathrm{T_{ek}}$ present the torque of $\mathrm{M_k}$ involved in a MIMPMSM system. The corresponding constrain on $|\mathrm{V}|$ is extended to be

$$\boldsymbol{|V| \ge \frac{Z}{N_p\varphi_p}\max\left\{|T_{eM_2} - T_e^n|, \cdots, |T_{eM_N} - T_e^n|\right\}} \tag{15}$$

which means that $|\mathrm{V}|$ must be determined with respect to the machine whose $\mathrm{T_e}$ owns the maximum distance to $\mathrm{T_e^n}$.

C. Steady-State Stability of the Open-Loop Machine

To analyze the stability of the open-loop machine, their linearized model can be used. The small signal model of PMSM around the steady-state has been presented in [31], which is

$$\begin{aligned}
\frac{dI_{dk}}{dt} &= -\frac{R_s}{L_s}I_{dk} + (\omega_e + \omega_{\delta k})\, I_{qk} - \frac{|V|\sin\delta_k}{L_s} \\
\frac{dI_{qk}}{dt} &= -(\omega_e + \omega_{\delta k})\, I_{dk} - \frac{R_s}{L_s}I_{qk} \\
&\quad + \frac{|V|\cos\delta_k}{L_s} - \frac{(\omega_e + \omega_{\delta k})\,\varphi_p}{L_s} \\
\frac{d\omega_k}{dt} &= \frac{{N_p}^2 I_{qk}\varphi_p - f_k(\omega_e + \omega_{\delta k}) - T_{lk}}{J_k} \\
\frac{d\delta_k}{dt} &= -\omega_{M_k}
\end{aligned} \tag{16}$$

where f is the viscous friction coefficient, J is the moment of inertia. It has such form

$$\boldsymbol{\dot{x} = f(x, u)} \tag{17}$$

with

$$\boldsymbol{x = \left[I_{dk}\ I_{qk}\ \omega_k\ \omega_{\delta k}\right]^T} \tag{18}$$

representing the dynamics of the open-loop machine $\mathrm{M_k}, \mathrm{k} \in [2, \mathrm{N}]$. The linearized system equations of this nonlinear system have the form

$$\boldsymbol{\Delta\dot{x} = A(x_0)\,\Delta x + B(x_0)\,\Delta u} \tag{19}$$

with

$$\boldsymbol{x_0 = \left[0\ \frac{T_{e0}}{N_p\varphi_p}\ \omega_{e0}\ 0\right]^T} \tag{20}$$

and

$$\boldsymbol{A}(\boldsymbol{x}_0)=\begin{bmatrix} -\frac{\boldsymbol{R_s}}{\boldsymbol{L_s}} & \boldsymbol{\omega}_{e0} & \frac{\boldsymbol{T}_{e0}}{\boldsymbol{N_p\varphi_p}} & -\frac{\boldsymbol{V_q}}{\boldsymbol{L_s}} \\ -\boldsymbol{\omega}_{e0} & -\frac{\boldsymbol{R_s}}{\boldsymbol{L_s}} & -\frac{\boldsymbol{\varphi_p}}{\boldsymbol{L_s}} & \frac{\boldsymbol{V_d}}{\boldsymbol{L_s}} \\ 0 & \frac{\boldsymbol{{N_p}^2\varphi_p}}{\boldsymbol{J}} & -\frac{\boldsymbol{f_k}}{\boldsymbol{J}} & 0 \\ 0 & 0 & -1 & 0 \end{bmatrix} \tag{21}$$

Fig. 4 shows the eigenvalues of (28) under different speed conditions based on the parameters of the experiment machine. The $|\mathrm{V}|$ is calculated by (5). It can be concluded that the open-loop machine is stable under the given condition.

D. Implementation of the Control Strategy

The proposed control strategy is designed based on the current FOC control that closed-loop control $\mathrm{I_d}$ and $\mathrm{I_q}$ of the master machine. Equation (15) has given out the synchronization condition with respect to the voltage amplitude. It must be converted to a constrain on $\mathrm{I_{d1}^*}$ as it is the control variable. Now the control method start calculating each open-loop machine's corresponding valid range of $\mathrm{I_{d1}^*}$ and apply the value in the intersection range to achieve the synchronization condition. The valid $\mathrm{I_{d1}}$ range of anyone of open-loop machine $\mathrm{M_k}, \mathrm{k}\in[2,\mathrm{N}]$ is given by (25) directly. Its detailed derivation can be found in Appendix B. The evaluation function expressed by $\mathrm{f}(\mathrm{T_e},\omega_\mathrm{e})$ is

$$\boldsymbol{f}\ (\boldsymbol{T_e},\boldsymbol{\omega_e})=\left(\frac{1}{\boldsymbol{N_p\varphi_p}}\right)^2\boldsymbol{T_e}\left(\boldsymbol{T_e}-2\boldsymbol{T_e^n}\right) \tag{22}$$

which evaluates the "distance" to $\mathrm{T_e^n}$, the higher $\mathrm{f}(\mathrm{T_e},\omega_\mathrm{e})$, the "more loaded" (include motor and braking mode) is the machine. Based on (25) two control strategies are designed. Their control schemes are shown in Fig. 5.

1) Extended Master Selection Strategy: The first control strategy is an extension of *master–slave* strategy. The working procedure during each control instant is as follows:

1) Calculate the evaluation value of each open-loop machine using (22).
2) Choose the machine with the highest value as the master ($\mathrm{M_1}$).

Refer to (25), $\mathrm{I_{d1}^*}\in(-\infty,+\infty)$ under this condition. $\mathrm{I_{d1}^*}$ is then regulated to 0 or an optimal $\mathrm{I_{d1}^*}$ to achieve the MTPA condition, which has been described in the last section.

This control strategy extends the master–slave strategy to braking mode. Because in the original version, the machine with higher load torque is selected as the master. Its selection logic is

$$\boldsymbol{\theta_{e1}}\left\langle\boldsymbol{\theta_{e1}}\Leftrightarrow\boldsymbol{\delta_1}\right\rangle\boldsymbol{\delta_1}\Leftrightarrow\boldsymbol{T_{e1}}>\boldsymbol{T_{e1}}. \tag{23}$$

When $\theta_{\mathrm{e1}}<\theta_{\mathrm{e1}}$, which equals to $\mathrm{T_{e1}}>\mathrm{T_{e1}}$, $\mathrm{M_1}$ is selected as the master, and vice versa. This logic is a special case of (22) when all machines' torque is larger than $\mathrm{T_e^n}$ as

$$\boldsymbol{f}\left(\boldsymbol{T_{e1}},\boldsymbol{\omega_e}\right)\left\langle\boldsymbol{f}\left(\boldsymbol{T_{e2}},\boldsymbol{\omega_e}\right)\Leftrightarrow\boldsymbol{T_{e1}}\right\rangle\boldsymbol{T_{e2}}>\boldsymbol{T_e^n}. \tag{24}$$

When anyone of the machine's torque is less than $\mathrm{T_e^n}$, (23) is no longer valid and leads to a wrong selection of the master machine.

2) Nonmaster Selection Strategy: As shown in Fig. 5(b), the controller structure contains a dedicated block that is responsible for calculating appreciate $\mathrm{I_{d1}^*}$. The machine under control remains unchanged. The working procedure during each control instant is as follows.

1) Calculate the evaluation value of each machine using (22).
2) Choose the machine with the highest evaluation value and use (25) shown at the bottom of this page, to calculate the valid range of $\mathrm{I_{d1}^*}$.
3) If MTPA point regulation is not applied, then $\mathrm{I_{d1}^*}$ is set to the minimal magnitude value in (25). Otherwise, the obtained optimal $\mathrm{I_{d1}^*}$ is set.

E. Calculation of MTPA Point

In this article, the MTPA condition of a MIMPMSM taking joule loss into account is considered. The joule loss mainly occurs on the stator windings, which is described as

$$\mathbf{joule\,loss}=\boldsymbol{R_s}\left(\boldsymbol{{I_{d1}}^2}+\boldsymbol{{I_{q1}}^2}\right)+\cdots+\boldsymbol{R_s}\left(\boldsymbol{{I_{dN}}^2}+\boldsymbol{{I_{qN}}^2}\right). \tag{26}$$

Thus, the cost function is defined as

$$\boldsymbol{f}\ (\boldsymbol{I_{d1}},\ldots,\boldsymbol{I_{dN}})=\boldsymbol{{I_{d1}}^2}+\cdots+\boldsymbol{{I_{dN}}^2} \tag{27}$$

to be minimized by the MTPA algorithm. Considering that for a MIMPMSM system, all machines share the same voltage, thus (28) can be applied between $\mathrm{M_1}$ and $\mathrm{M_k}, \mathrm{k}\in[2,\mathrm{N}]$

$$\boldsymbol{{V_{d1}}^2}+\boldsymbol{{V_{q1}}^2}=\boldsymbol{{V_{dk}}^2}+\boldsymbol{{V_{qk}}^2}. \tag{28}$$

Insert (1) and (3) into (28), the expression of $\mathrm{I_{dk}}$ can be obtained

$$\boldsymbol{Z}^2\boldsymbol{{I_{dk}}^2}+\boldsymbol{\alpha}\boldsymbol{I_{dk}}+\boldsymbol{\beta}=0 \tag{29}$$

where

$$\boldsymbol{\alpha}=2\boldsymbol{L_s}\boldsymbol{{\omega_e}^2}\boldsymbol{\varphi_p} \tag{30}$$

$$\begin{aligned}\boldsymbol{\beta}=&\left(\boldsymbol{\omega_e}\boldsymbol{L_s}\boldsymbol{I_{qk}}\right)^2+\left(\boldsymbol{R_s}\boldsymbol{I_{qk}}+\boldsymbol{\omega_e}\boldsymbol{\varphi_p}\right)^2\\&-\left(\boldsymbol{R_s}\boldsymbol{I_{d1}}-\boldsymbol{L_s}\boldsymbol{\omega_e}\boldsymbol{I_{q1}}\right)^2-\left(\boldsymbol{R_s}\boldsymbol{I_{q1}}+\boldsymbol{L_s}\boldsymbol{\omega_e}\boldsymbol{I_{d1}}+\boldsymbol{\omega_e}\boldsymbol{\varphi_p}\right)^2.\end{aligned} \tag{31}$$

Treat (29) as a constraint of each machine, that is

$$\boldsymbol{g_k}\left(\boldsymbol{I_{d1}},\boldsymbol{I_{dk}}\right)=\boldsymbol{Z}^2\boldsymbol{{I_{dk}}^2}+\boldsymbol{\alpha}\boldsymbol{I_{dM_k}}+\boldsymbol{\beta} \tag{32}$$

the Lagrange multiplier can be designed as

$$\boldsymbol{I_{d1}^*}\in\begin{cases}\left(-\infty,\ -\frac{\boldsymbol{L_s}\boldsymbol{{\omega_e}^2}\boldsymbol{\varphi_p}}{\boldsymbol{Z}^2}-\sqrt{\boldsymbol{f}\left(\boldsymbol{T_{ek}},\boldsymbol{\omega_e}\right)-\boldsymbol{f}\left(\boldsymbol{T_{e1}},\boldsymbol{\omega_e}\right)}\right]\cup\left[-\frac{\boldsymbol{L_s}\boldsymbol{{\omega_e}^2}\boldsymbol{\varphi_p}}{\boldsymbol{Z}^2}+\sqrt{\boldsymbol{f}\left(\boldsymbol{T_{ek}},\boldsymbol{\omega_e}\right)-\boldsymbol{f}\left(\boldsymbol{T_{e1}},\boldsymbol{\omega_e}\right)}\ ,\ +\infty\right) & \boldsymbol{f}\left(\boldsymbol{T_{ek}},\boldsymbol{\omega_e}\right)>\boldsymbol{f}\left(\boldsymbol{T_{e1}},\boldsymbol{\omega_e}\right)\\ (-\infty,+\infty) & \boldsymbol{f}\left(\boldsymbol{T_{ek}},\boldsymbol{\omega_e}\right)<\boldsymbol{f}\left(\boldsymbol{T_{e1}},\boldsymbol{\omega_e}\right)\end{cases} \tag{25}$$

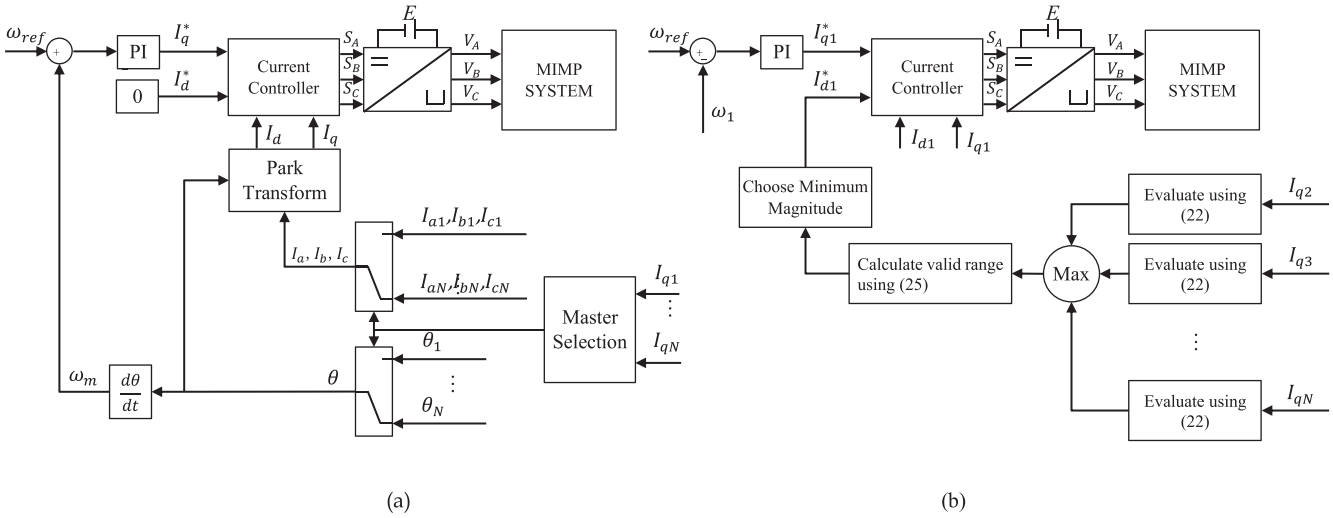

Fig. 5. Block diagram of proposed control scheme. (a) Nonmaster selection. (b) Master selection.

$$\boldsymbol{L}\left(\boldsymbol{I_{d1}}, \boldsymbol{\lambda_1}, \ldots, \boldsymbol{\lambda_N}\right) = \boldsymbol{f}\left(\boldsymbol{I_{d1}}, \ldots, \boldsymbol{I_{dN}}\right) + \sum_{\boldsymbol{i=2}}^{\boldsymbol{N}} \boldsymbol{\lambda_i g_i}\left(\boldsymbol{I_{d1}}, \boldsymbol{I_{di}}\right). \tag{33}$$

Performing partial differential to (33), the results can be divided into three parts as shown in (36)–(38). The solution of these equations contributes the candidates of the optimal efficiency point. The relationship between λ_i and I_{di} can be extracted through (37), which is

$$\boldsymbol{\lambda_i} = -\frac{2\boldsymbol{I_{di}}}{2\boldsymbol{Z}^2\boldsymbol{I_{di}} + \boldsymbol{\alpha}}, \boldsymbol{i} \in [2, \boldsymbol{N}]. \tag{34}$$

Then, according to (36) and (38), all λ can be eliminated. Equations with respect to I_{di} is shown in (35)

$$\begin{cases} \sum_{\boldsymbol{k}=1}^{\boldsymbol{N}} \frac{2\boldsymbol{I_{dk}}}{2\boldsymbol{Z}^2\boldsymbol{I_{dk}}+\boldsymbol{\alpha}} = 0 \\ \boldsymbol{Z}^2{\boldsymbol{I_{d2}}}^2 + \boldsymbol{\alpha I_{d2}} + \boldsymbol{\beta} = 0 \\ \qquad\qquad \vdots \\ \boldsymbol{Z}^2{\boldsymbol{I_{dN}}}^2 + \boldsymbol{\alpha I_{dN}} + \boldsymbol{\beta} = 0. \end{cases} \tag{35}$$

When $N = 1$, it is easy to identify that $\mathrm{I_{d1}} = 0$ is the solution. When $N = 2$, the result is the same as that in [14]. In the case of $N \geq 3$, this equation is no longer analytically solvable like the dual-PMSM cases presented in [13] and [14]. A numerical method must be used to obtain the solution

$$\begin{cases} \frac{\partial L(I_{d1},\ldots,I_{dN},\lambda_1,\ldots,\lambda_N)}{\partial I_{d1}} = 2I_{d1} \\ -\left(\lambda_2 + \ldots + \lambda_N\right)\left(2Z^2 I_{d1} + \alpha\right) = 0 \end{cases} \tag{36}$$

$$\begin{cases} \frac{\partial L(I_{d1},\ldots,I_{dN},\lambda_1,\ldots,\lambda_N)}{\partial I_{d2}} = 2I_{d2} + \lambda_{M_2}\left(2Z^2 I_{d2} + \alpha\right) = 0 \\ \vdots \\ \frac{\partial L(I_{d1},\ldots,I_{dN},\lambda_1,\ldots,\lambda_N)}{\partial I_{dN}} = 2I_{dN} + \lambda_{M_N}\left(2Z^2 I_{dN} + \alpha\right) = 0 \end{cases} \tag{37}$$

$$\begin{cases} \frac{\partial L\left(I_{d1},\ldots,I_{dN},\lambda_{M_1},\ldots,\lambda_{M_N}\right)}{\partial \lambda_2} = Z^2{I_{d2}}^2 + \alpha I_{d2} + \beta = 0 \\ \vdots \\ \frac{\partial L(I_{d1},\ldots,I_{dN},\lambda_1,\ldots,\lambda_N)}{\partial \lambda_N} = Z^2{I_{dN}}^2 + \alpha I_{dN} + \beta = 0. \end{cases} \tag{38}$$

F. Consideration of Parameter Variation

The proposed control strategies, especially the evaluation function (22), depend on the parameters' correctness. When machines' parameters change during operation, (22) may give out distorted value. To increase the robustness, we proposed to apply an additional current in $I_{d1}$to compensate the parameter variation, because the criterion given by (25) determines the exact minimal voltage. An additional current in I_{d1} results in higher voltage, which make the control strategies more robust.

IV. Experiment Test

An experiment test was conducted in our lab to verify the feasibility and performance of the proposed controller. Fig. 6 shows the experimental bench. There are six machines involved in the experiment. Three of them are experiment PMSMs, and the other three are controllable torque-generator based on dc machines. The sensor sampling and current control command loop runs at 10 kHz.

A dedicated triple-PMSM control board (see Fig. 7) that consists of a main controller, an inverter, six current sensors, three encoder ports is designed and manufactured to conduct the experiment. Their types are indicated in Table II. Each machine is equipped with an encoder and two hall current sensors, which measure the current on phase A and B. This control board has integrated an SD card slot so all experiment data can be stored in it.

A battery is connected parallel to the dc bus so as to keep the dc bus voltage stable, as there is energy circulation between the

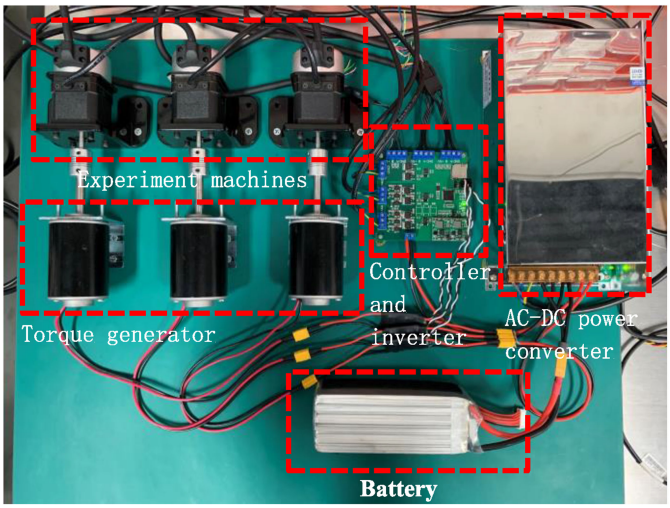

Fig. 6. Experiment bench.

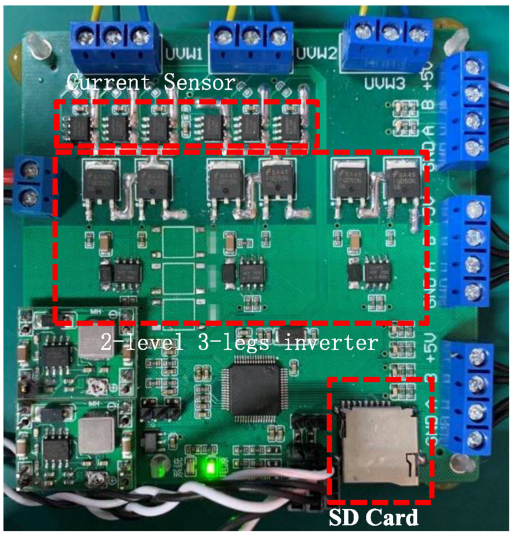

Fig. 7. Designed and manufactured controller.

TABLE I PARAMETERS OF THE EXPERIMENT MACHINE

Symbol	Description	Value
V_{dc}	Voltage of the DC bus	24 V
I_n	Nominal current	1.8 A
P_n	Nominal power	32 W
ω_n	Nominal Speed	3000 RPM
R_s	Stator phase resistance	1.2 Ω
L_s	Stator phase inductance	0.6 mH
φ_p	Amplitude of the flux due to the magnets	1.42×10^{-2} V/rad
N_p	Number of pairs of poles	4
f	Viscous friction coefficient	3.3×10^{-6} N · m/Rad
J	Moment of inertia (including the load)	1.3×10^{-5} kg · m^2

TABLE II PARAMETERS OF THE CONTROL BOARD

Name	Type
Main Controller	STM32F405RGT6
Current Sensor	CC6904SO-20A
Power switch	FQD50N06
MOS driver	IR2101S
Encoder pules	2048 pules/round
Current control frequency	10 kHz
Speed control frequency	1 kHz

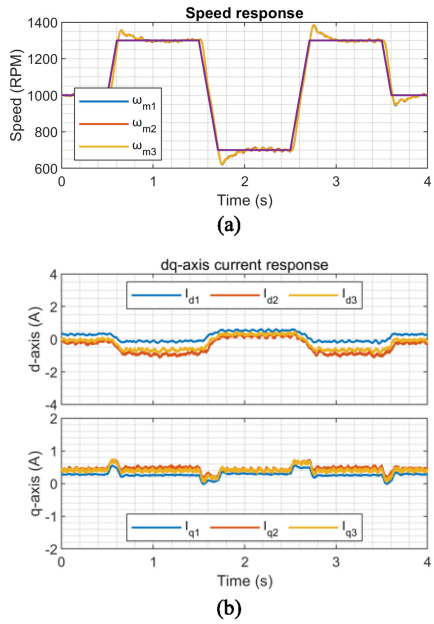

Fig. 8. Speed transient experiment result of nonmaster selection strategy.

experimental machines and the torque generator. For example, when in motor mode, the experiment machines are absorbing energy while the torque generators are generating power, as their power switching timing is not synchronized and the ac–dc power module is monodirectional, the dc bus voltage will rise when the system is generating power.

In the experiment, a regular PI-based FOC controller is responsible for controlling the current of the master machine. They are tuned with the help of the simulation model built in the MATLAB/Simulink and the PID tune function in the control toolbox.

The machine parameters are shown in Table I. The experiment is divided into three parts: speed transient, motor starting, load torque, and efficiency optimization.

A. *Speed Transient Test*

Figs. 8 and 9 show the speed transient experiment results of two control strategies. A ramp-shaped speed reference with 300 rad/s^2 acceleration limitation is given. Both can perform well during speed transient situations. All machines are fully

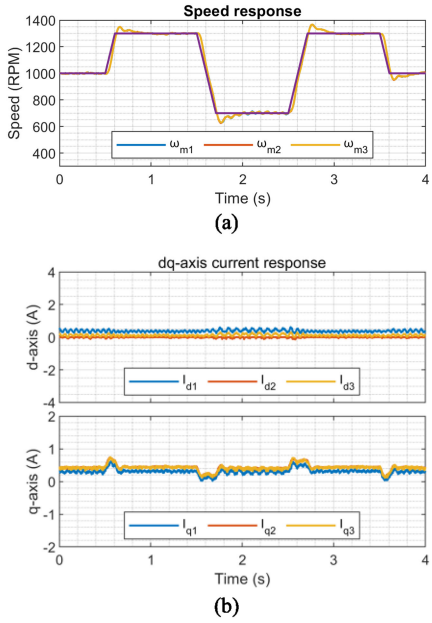

Fig. 9. Speed transient experiment result of extended master selection strategy.

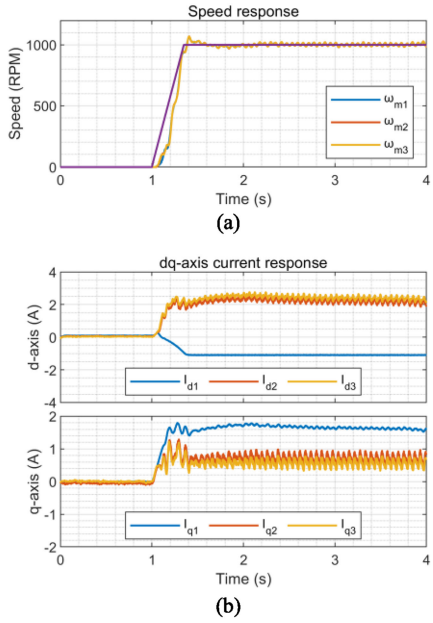

Fig. 10. Motor starting experiment result of nonmaster selection strategy-$\mathbf{M}_1$ is the most loaded.

synchronized so that little speed difference can be observed from the response. The overshoot in the response is caused by the underdamping characteristic of the system, as there is no damping device connecting to the experiment machines.

B. Motor Starting Test

This test mainly focuses on the system's behavior when the machines' load is different during the starting phase. In the experiment, we have tested both two control strategies under two situations, which corresponds to M_1 or M_2 is the most loaded machine, respectively. Figs. 10–13 illustrates the experiment results. The proposed strategies can start the system normally without knowing the torque relationship in prior.

C. Unbalanced Load Torque Test

The proposed two control strategies depend heavily on torque relationship determination. The nonmaster-selection strategy must use the torque relationship of each machine to determine the value range of I_{d1}. The extended master-selection strategy must use it to determine the master machine. To verify the correctness of the control strategies, this experiment is divided into two parts: motor mode and brake mode. In motor mode, the machines are brought to steady speed operation condition. Then, each machine is assigned an external load torque so that we can have a relationship transition of each machine. For the brake mode, we must consider that the corresponding I_q^n of $\mathrm{T_e^n}$ under given operating condition is

$$\boldsymbol{I_q^n = -\frac{R_s \omega_e \varphi_p}{Z^2}} \tag{39}$$

which is proportional to the speed. Thus, we must use a relatively low speed (500 round per minute) so that the total current would

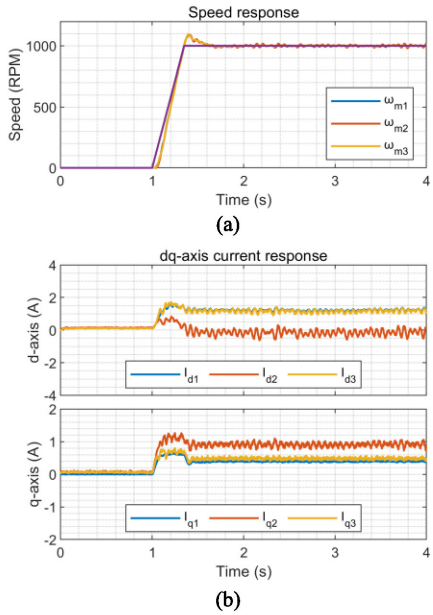

Fig. 11. Motor starting experiment result of nonmaster selection strategy-$\mathbf{M}_2$ is the most loaded.

not exceed the machines' current limit too much. Under such condition, the corresponding $I_q^n = -2.44$ A.

Fig. 14 has shown the experiment results of the nonmaster selection strategy in motor mode. Fig. 14(a) shows the speed response, Fig. 14(b) shows the current response in *d-q* coordinate. Fig. 14(c) shows the motor's phase current and inverter's current. Here, we only present phase-A's current. Fig. 14(d) shows the voltage reference in M_1's frame. Around 1.4 s, M_1 becomes

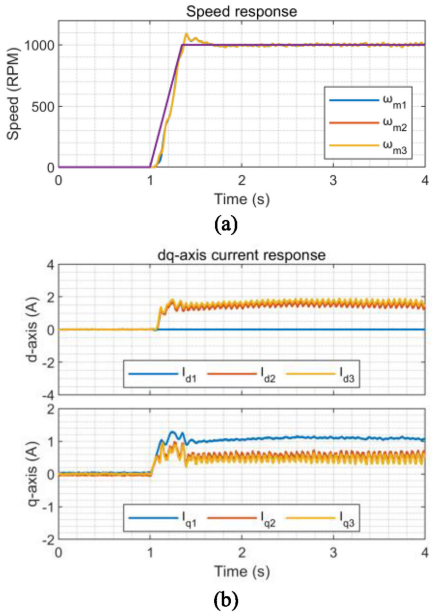

Fig. 12. Motor starting experiment result of the extend master selection strategy-M_1 is the most loaded.

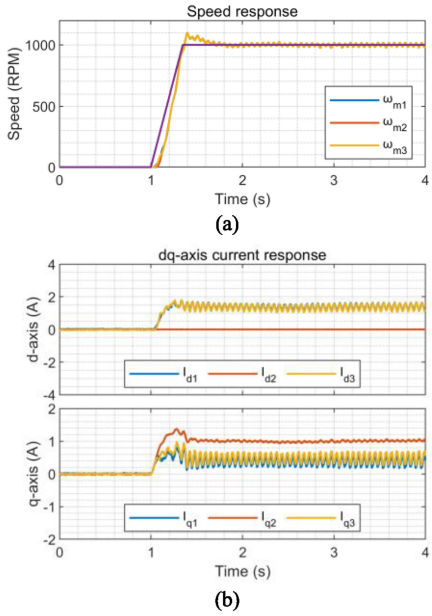

Fig. 13. Motor starting experiment result of the extend master selection strategy-M_2 is the most loaded.

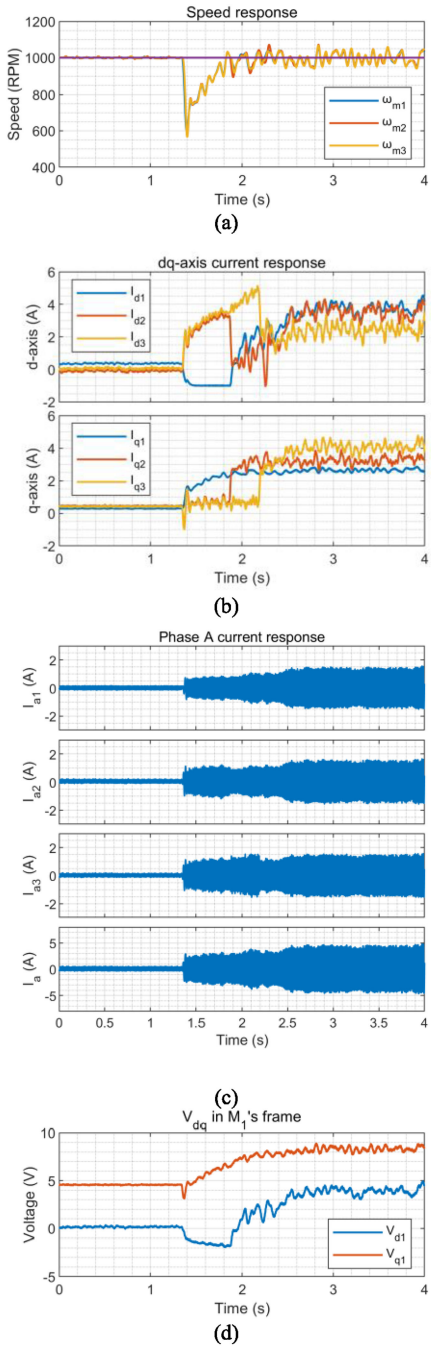

Fig. 14. Experiment result of nonmaster selection strategy in motor mode

the most loaded machine. Refer to (25), the value range of $\mathrm{I}_{\mathrm{dM}_1}$ is $(-\infty, +\infty)$. Thus, in such condition, $\mathrm{I}_{\mathrm{dM}_1}$ (blue curve) is regulated as $-\frac{L_s {\omega_e}^2 \varphi_p}{Z^2} + \underbrace{0.1\mathrm{A}}_{\text{compensation current}} \approx -1\mathrm{A}$. The system's stability is kept.

Around 1.8 s, M_2 becomes the most loaded machine. I_{d1} increases immediately to preserve the system stability following the constraint applied by (25). The same transition happens to M_3 as its applied torque increases. The system is still stable even without master selection.

Fig. 15 shows the response in brake mode. The red dash line in Fig. 15(b) represents I_q^n. After 1.6 s, all machines' q-axis current is below this line indicating that they are in brake mode. Again, the load torque transition makes M_2 and M_3 become the most loaded machine one by one. Thanks

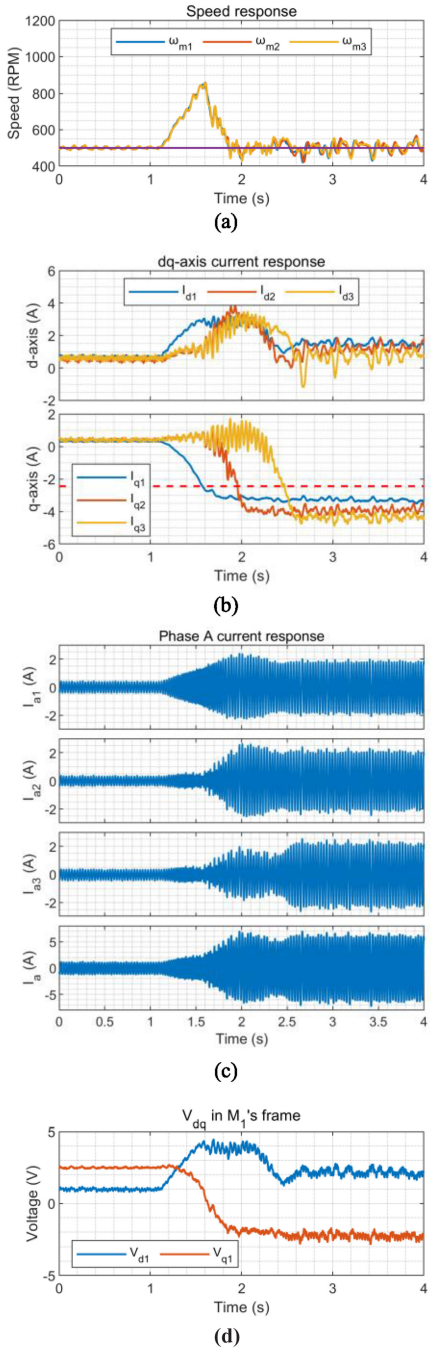

Fig. 15. Experiment result of nonmaster selection strategy in brake mode.

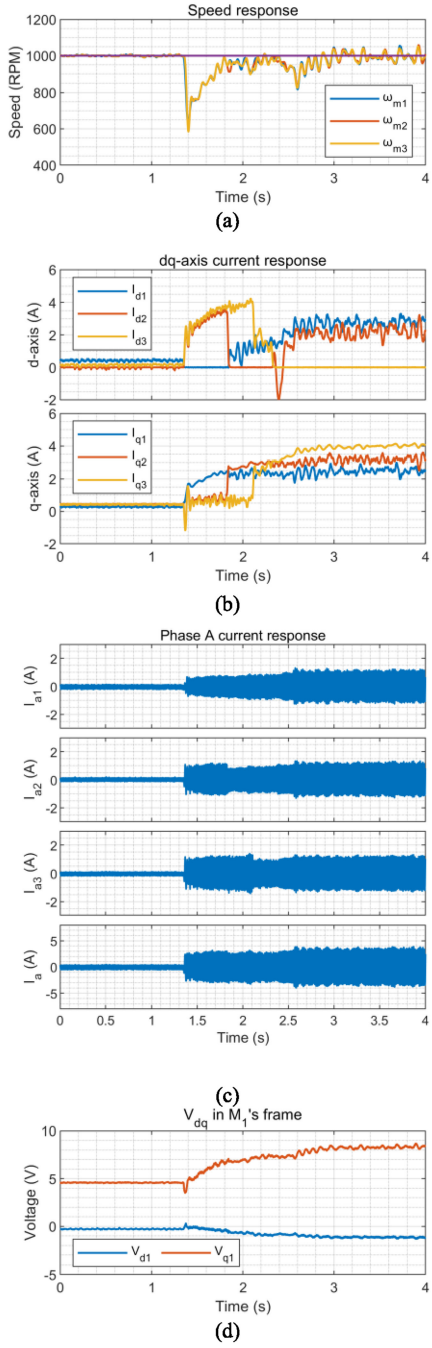

Fig. 16. Experimental result of extend master selection strategy in motor mode.

to the correct regulated I_{d1}, the system can preserve the stability.

Fig. 16 illustrates the result of the extended master-selection strategy in motor mode. The experiment configuration is the same as it is for nonmaster selection strategy. When there is no external load applied, I_{d1} is also regulated as 0. The only difference is that when a machine becomes the most loaded, its I_d becomes 0.

Fig. 16 has proven that the extended master-selection strategy can also handle the machines in brake mode.

D. *Efficiency Optimization*

As the numerical method is too complex to run inside a microcontroller in real time, at this stage, we have used an offline method that calculate the optimal I_{d1}^* and applied during experiment. The experiment configuration is the same as the motor mode test in the unbalanced load torque test. The efficiency result is shown in Fig. 18. The blue and red curves represent the efficiency of the original nonmaster selection strategy and extend

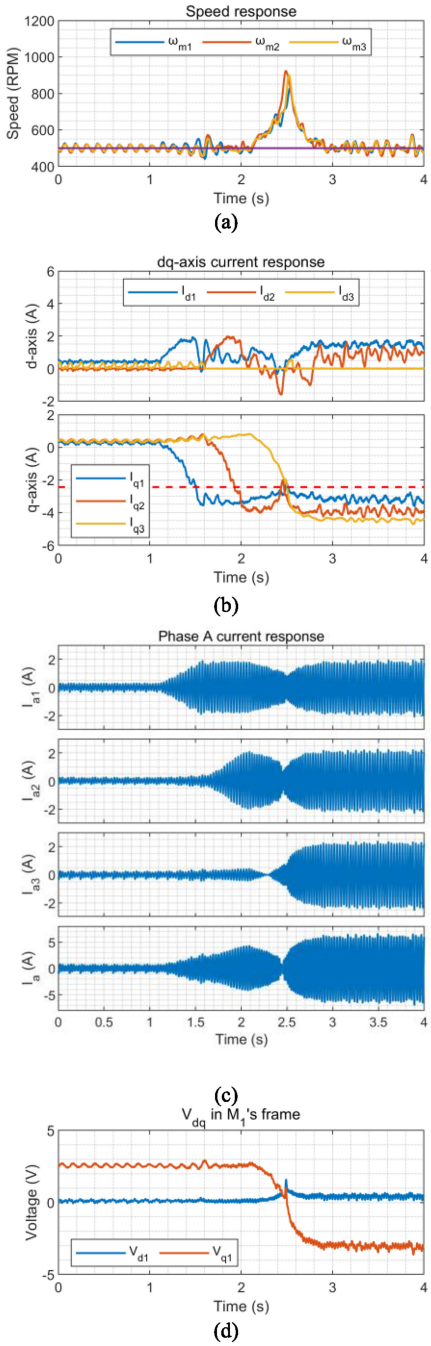

Fig. 17. Experimental result of extend master selection strategy in brake mode.

master-selection strategy, respectively. The yellow one is the nonmaster selection strategy with optimization. Their effciency is calculated by

$$\eta = \frac{\omega_e \varphi_p \sum_{k=1}^{4} I_{qM_k}}{\omega_e \varphi_p \sum_{k=1}^{4} I_{qM_k} + R_s \sum_{k=1}^{4} \left(I_{dM_k}^2 + I_{qM_k}^2\right)}. \tag{40}$$

It can be concluded that the effectiveness of the efficiency optimization is obvious especially when torques are highly imbalanced.

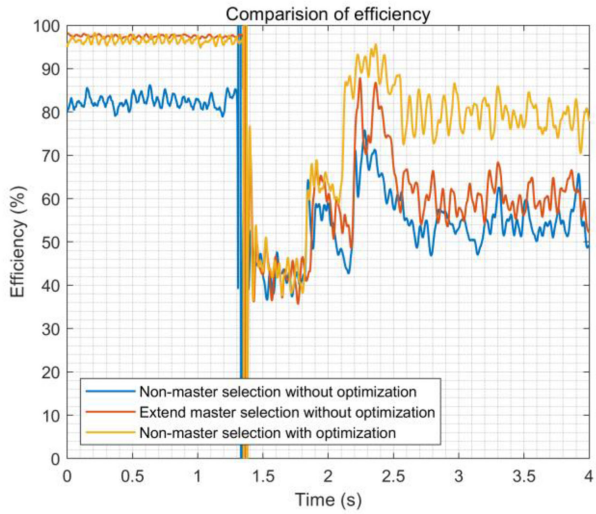

Fig. 18. Efficiency comparison between strategies.

V. Conclusion

In this article, we have proposed two control strategies to a MIMPMSM system containing more than two machines. By using the constraint analysis method, it is proved that the MIMPMSM system is feasible. Like the MIDPMSM system, the controller must and can only control one extra variable to make the system fully constrained.

Then, based on the open-loop stability of a PMSM, the stability criterion of a MIMPMSM system is derived. One must provide enough voltage which takes speed, torque into consideration to preserve the stability of the system. Refer to this criterion, two control strategies are designed. Both only control one machine among all machines. The first strategy, called nonmaster-selection, regulates $\mathrm{I_{dM_1}}$ passively under the constraints to assure the system stability. On the other hand, in the master-selection strategy, we calculate the value of the function (22) and choose the machine with the highest value as the master. This strategy extends the conventional master-slave strategy to brake mode, which makes sense in traction applications such as an electric vehicle.

Meanwhile, the efficiency optimization method is also extended to an MIMPMSM system. With this process, the optimal operation point minimizing the joule losses is obtained.

Finally, we have verified these control strategies in an extensive experiment involving three machines. The experiment results verify that both control strategies are operational and stable, which proves the correctness of the controller design method proposed in this article. They can start the motors normally even highly unbalanced torques applied. Moreover, these strategies can work not only in motor mode but also in brake mode. The efficiency comparison test has shown a great performance advantage compared to a traditional MTPA law.

This article also raises many problems, such as the impact of parameter variation on system stability and efficiency optimization, the possibility in improving the dynamic performance, lack of an effective algorithm to solve the optimization problem so

that it can run in real time in a microcontroller. These problems remain to be solved in future studies.

APPENDIX

A. Power Neutral Point of a PMSM

T_e^n corresponds to the braking torque when zero voltage is applied. In such a condition, the three-phase terminations are connected in short circuit. It can be easily obtained by setting the voltage in (1) equals to zero, which is

$$\begin{bmatrix} 0 \\ 0 \end{bmatrix} = \begin{bmatrix} R_s & -L_s\omega_e \\ L_s\omega_e & R_s \end{bmatrix} \begin{bmatrix} I_d \\ I_q \end{bmatrix} + \begin{bmatrix} 0 \\ \omega_e\varphi_p \end{bmatrix}. \tag{41}$$

The corresponding currents can be calculated. They are

$$\begin{cases} I_d = -\frac{L_s{\omega_e}^2\varphi_p}{Z^2} \\ I_q = -\frac{R_s\omega_e\varphi_p}{Z^2}. \end{cases} \tag{42}$$

The torque is

$$T_e = N_p\varphi_p I_q = -N_p\varphi_p\frac{R_s\omega_e\varphi_p}{Z^2} \tag{43}$$

that is exactly the same as $\mathrm{T_e^n}$. The effective power can be expressed as

$$\begin{aligned} \vec{V}_{dq}\cdot\vec{I}_{dq} &= \left|\vec{V}_{dq}\right|\left|\vec{I}_{dq}\right|\cos\varphi \\ &= \underbrace{R_s\left({I_d}^2+{I_q}^2\right)}_{Power\,on\,resistance} + \underbrace{\omega_e\varphi_p I_q}_{Mechanical\,power} \end{aligned} \tag{44}$$

where $\cos\varphi$ is the power factor. Equation (44) equals to zero because $\tilde{\mathrm{V}}_{\mathrm{dq}} = 0$. This means that all mechanical power is absorbed by stator resistance in such a condition.

B. Valid Range of $\boldsymbol{I_{d1}}$

Making square on both sides of (5), we can obtain

$$|V|^2\sin^2\delta = \left(R_sI_{d1} - L_s\omega_eI_{q1}\right)^2 \tag{45}$$

$$|V|^2\cos^2\delta = \left(R_sI_{q1} + L_s\omega_eI_{d1} + \omega_e\varphi_p\right)^2 \tag{46}$$

Add (45) onto (46), and replace $|\mathrm{V}|$ in (15), the inequation becomes

$$\begin{aligned} &Z^2\left({I_{d1}}^2+{I_{q1}}^2\right) + 2L_s\omega_e\omega_e\varphi_pI_d + \left(\omega_e\varphi_p\right)^2 + 2R_sI_q\omega_e\varphi_p \\ &\geq \left(\frac{Z}{N_p\varphi_p}\right)^2\left(T_{eM_{\max}} - T_e^n\right)^2. \end{aligned} \tag{47}$$

$\mathrm{T_{eM_{max}}}$ corresponds to the torque of the most loaded machine. Equation (49) is a quadratic inequation with respect to $\mathrm{I_{d1}}$. In order to obtain the solution, its discriminant must be discussed, which is

$$\Delta = 4Z^4\left(f\left(T_{e1},\omega_e\right) - f\left(T_{eM_{\max}},\omega_e\right)\right) \tag{48}$$

where

$$f\left(T_e,\omega_e\right) = -\left(\frac{1}{N_p\varphi_p}\right)^2\left({T_e}^2 - 2T_e^nT_e\right). \tag{49}$$

1) $\boldsymbol{T_{e1} = T_{eM_{max}}}$: When $\mathrm{T_{eM_1}} = \mathrm{T_{eM_{max}}}$, which means $\mathrm{M_1}$ is the most loaded machine, $\Delta = 0$ and the solution of (49) is $(-\infty, +\infty)$.

2) $\boldsymbol{T_{eM_1} < T_{eM_{max}}}$: $\mathrm{M_1}$ is not the most loaded machine. Because $\mathrm{f(T_e,\omega_e)}$ is a quadratic function opening downward and symmetrical to $\mathrm{T_e^n}$, for $\mathrm{T_{eM_1}} < \mathrm{T_{eM_{max}}}$ there must be $\mathrm{f(T_{eM_1},\omega_e)} > \mathrm{f(T_{eM_{max}},\omega_e)}$, which leads to $\Delta > 0$ and the solution of (49) is

$$\begin{aligned} &\left(-\infty, -\frac{L_s{\omega_e}^2\varphi_p}{Z^2} - \sqrt{f\left(T_{eM_1},\omega_e\right) - f\left(T_{eM_{\max}},\omega_e\right)}\right] \\ &\bigcup\left[\frac{-(L_s{\omega_e}^2\varphi_p)}{Z^2} + \sqrt{(f(T_{(eM_1)},\omega_e) - f(T_{(eM_max)},\omega_e))}, +\infty\right). \end{aligned} \tag{50}$$

ACKNOWLEDGMENT

The work presented in this article was realized during the PhD studying of the author Dr. Tianyi Liu in LAboratoire PLAsma et Conversion d'Energie (LAPLACE) in Nationale Supérieure d'Electrotechnique, d'Electronique, d'Informatique, d'Hydraulique et des Télécommunications, Institut National Polytechnique de Toulouse within the group COmmande et DIAgnostic des Systèmes Electriques. Authors would also like to thank to the China Scholarship Council (CSC) who has given the financial support during the Ph.D. studying, and Prof. Maurice Fadel, for the confidence, guidance, encouragement, and support.

REFERENCES

[1] P. Ghani, M. Arasteh, and H. R. Tayebi, "Analysis of electromechanical model of traction system with single inverter dual induction motor," in *Proc. 7th Power Electron. Drive Syst. Technol. Conf.*, Tehran, Iran, 2016, pp. 99–104.

[2] P. M. Kelecy and R. D. Lorenz, "Control methodology for single inverter, parallel connected dual induction motor drives for electric vehicles," in *Proc. Power Electron. Specialist Conf.*, Taipei, Taiwan, 1994, pp. 987–991.

[3] X. Xu, G. Zhou, J. Rao, and G. Yang, "Study and design of low-speed direct-driven permanent magnet synchronous machines (PMSM) for fan used on power air cooling island," in *Proc. 20th Int. Conf. Elect. Mach. Syst.*, Sydney, NSW, Australia, 2017, pp. 1–5.

[4] M. Dubey, S. Sharma, and R. Saxena, "Solar power based water pump employing Z-source inverter for PMSM drive," in *Proc. 8th IEEE India Int. Conf. Power Electron.*, Jaipur, India, 2018, pp. 1–5.

[5] P. D. C. Perera, F. Blaabjerg, J. K. Pedersen, and P. Thogersen, "A sensorless, stable v/f control method for permanent-magnet synchronous motor drives," *IEEE Trans. Ind. Appl.*, vol. 39, no. 3, pp. 783–791, May 2003.

[6] J. M. Lazi, Z. Ibrahim, M. H. N. Talib, and R. Mustafa, "Dual motor drives for PMSM using average phase current technique," in *Proc. IEEE Int. Conf. Power Energy*, Kuala Lumpur, 2010, pp. 786–790.

[7] A. Asri, D. Ishak, S. Iqbal, and M. Kamarol, "A speed sensorless field oriented control of parallel- connected dual PMSM," in *Proc IEEE Int. Conf. Control Syst., Comput. Eng.*, Penang, 2011, pp. 567–570.

[8] M. S. D. Acampa, A. Del Pizzo, and D. Iannuzzi, "Optimized control technique of single inverter dual motor AC-brushless drives," in *Proc. 43rd Int. Univ. Power Eng. Conf.*, Padova, Italy, 2008, pp. 1–6.

[9] A. Del Pizzo, D. Iannuzzi, and I. Spina, "High performance control technique for unbalanced operations of single-VSI dual-PM brushless motor drives," in *Proc. IEEE Int. Symp. Ind. Electron.*, Bari, 2010, pp. 1302–1307.

[10] Z. Deng and X. Nian, "Robust control of two parallel-connected permanent magnet synchronous motors fed by a single inverter," *IET Power Electron.*, vol. 9, no. 15, pp. 2833–2845, Dec. 2016.

[11] G. Brando, L. Piegari, and I. Spina, "Simplified optimum control method for monoinverter dual parallel PMSM drive," *IEEE Trans. Ind. Electron.*, vol. 65, no. 5, pp. 3763–3771, May 2018.

[12] D. Bidart, M. Pietrzak-David, P. Maussion, and M. Fadel, "Mono inverter multi-parallel permanent magnet synchronous motor: Structure and control strategy," *IET Elect. Power Appl.*, vol. 5, no. 3, pp. 288–294, Mar. 2011.

[13] T. Liu and M. Fadel, "An efficiency-optimal control method for mono-inverter dual-PMSM systems," *IEEE Trans. Ind. Appl.*, vol. 54, no. 2, pp. 1737–1745, Mar./Apr. 2018.

[14] Y. Lee and J.-I. Ha, "Control method for mono inverter dual parallel surface-mounted permanent-magnet synchronous machine drive system," *IEEE Trans. Ind. Electron.*, vol. 62, no. 10, pp. 6096–6107, Oct. 2015.

[15] T.-I. Yeam and D.-C. Lee, "Speed control of single inverter dual PMSM drives using sliding mode control," in *Proc IEEE Veh. Power Propul. Conf.*, Vietnam, Oct. 2019, pp. 1–6.

[16] M. S. D. Acampa, A. Del Pizzo, D. Iannuzzi, and I. Spina, "Predictive control technique of single inverter dual motor AC-brushless drives," in *Proc. 18th Int. Conf. Elect. Mach.*, Vilamoura, 2008, pp. 1–6.

[17] N. L. Nguyen, M. Fadel, and A. Llor, "A new approach to predictive torque control with dual parallel PMSM system," in *Proc. IEEE Int. Conf. Ind. Technol.*, 2013, pp. 1806–1811.

[18] A. Bouarfa and M. Fadel, "Optimal predictive torque control of two PMSM supplied in parallel on a single inverter," in *Proc. 9th IFAC Symp. Control Power Energy Syst.*, New Delhi, 2015, vol. 48, pp. 84–89.

[19] T. Liu and M. Fadel, "Performance comparison of control strategies for mono-inverter dual-PMSM system," in *Proc. IEEE Int. Power Electron. Motion Control Conf.*, Varna, 2016, pp. 637–642.

[20] T. Liu and M. Fadel, "Comparative study of different predictive torque control strategies for mono-inverter dual-PMSM system," in *Proc. 18th Mediterranean Electrotech. Conf.*, Lemesos, 2016, pp. 1–6.

[21] Y. Yamada, T. Nozaki, and T. Murakami, "Independent drive of multiple ac motors using amplitude modulation," in *Proc. IEEE Int. Conf. Ind. Technol.*, Buenos Aires, Argentina, 2020, pp. 181–186.

[22] T. Nagano, G. T. Chiang, and J. Itoh, "Parallel connected multiple motor drive system using small auxiliary inverter for permanent magnet synchronous motors," *IEE J. Ind. Appl.*, vol. 4, no. 1, pp. 40–48, 2015.

[23] T. Liu, M, and Fadel, "A controller proposed for mono-inverter multiple-PMSM system," in *Proc. 20th IFAC World Congr.*, vol. 50, 2017, pp. 14800–14805.

[24] Y.-Chih Chang, J.-T. Chan, J.-C. Chen, and J.-G. Yang, "Development of permanent magnet synchronous brake drive in electrical vehicle power system," in *Proc. IEEE Veh. Power Propul. Conf.*, Seoul, South Korea, 2012, pp. 115–118.

[25] L. Vido, M. Ruellan, Y. Amara, H. Ben Ahmed, and G. Mohamed, "PMSM optimal parameters for a specification sheet including motor and brake operation," in *Proc. XIX Int. Conf. Elect. Mach.*, Rome, Italy, 2010, pp. 1–6.

[26] A. N. Reshetnikov and S. V. Klassen, "PMSM analysis in *dq* axis at brake mode as the part of ISG," in *Proc. 17th Int. Conf. Young Specialists Micro/Nanotechnol. Electron Devices*, Erlagol, 2016, pp. 536–538.

[27] K. Lee, J. Im, I. Choy, W. Cho, and J. Back, "MPPT and yawing control of a new horizontal-axis wind turbine with two parallel-connected generators," in *Proc. 8th Int. Conf. Power Electron.*, Jeju, 2011, pp. 2618–2624.

[28] D. S. Oliveira, M. M. Reis, C. E. A. Silva, L. H. S. Colado Barreto, F. L. M. Antunes, and B. L. Soares, "A three-phase high-frequency semicontrolled rectifier for PM WECS," *IEEE Trans. Power Electron.*, vol. 25, no. 3, pp. 677–685, Mar. 2010.

[29] J.-S. Kim and S.-K. Sul, "New approach for high-performance PMSM drives without rotational position sensors," *IEEE Trans. Power Electron.*, vol. 12, no. 5, pp. 904–911, Sep. 1997.

[30] R. S. Colby and D. W. Novotny, "An efficiency-optimizing permanent-magnet synchronous motor drive," *IEEE Trans. Ind. Appl.*, vol. 24, no. 3, pp. 462–469, May 1988.

[31] M. Novak and Z. Novak, "Stability issues of high-speed PMSM feedback control systems," in *Proc. 15th Eur. Conf. Power Electron. Appl.*. , Lille, 2013, pp. 1–9.